

Article

Not peer-reviewed version

Hypomagnetic Field Exposure Disrupts Iron–Sulfur Homeostasis and Oxidative Balance in a Frataxin-Deficient Insect System

Hui-Ming Kang , Bing Li , Shuai Yan , Li-Li Zhang , [Gui-Jun Wan](#) , [Jun-Zheng Zhang](#) , [Wei-Dong Pan](#) *

Posted Date: 28 January 2026

doi: 10.20944/preprints202601.2085.v1

Keywords: hypomagnetic field; frataxin; SR-XRF; iron/sulfur; oxidative stress



Preprints.org is a free multidisciplinary platform providing preprint service that is dedicated to making early versions of research outputs permanently available and citable. Preprints posted at Preprints.org appear in Web of Science, Crossref, Google Scholar, Scilit, Europe PMC.

Copyright: This open access article is published under a [Creative Commons CC BY 4.0 license](#), which permit the free download, distribution, and reuse, provided that the author and preprint are cited in any reuse.

Disclaimer/Publisher's Note: The statements, opinions, and data contained in all publications are solely those of the individual author(s) and contributor(s) and not of MDPI and/or the editor(s). MDPI and/or the editor(s) disclaim responsibility for any injury to people or property resulting from any ideas, methods, instructions, or products referred to in the content.

Article

Hypomagnetic Field Exposure Disrupts Iron–Sulfur Homeostasis and Oxidative Balance in a Frataxin-Deficient Insect System

Hui-Ming Kang ^{1,2}, Bing Li ^{1,2}, Shuai Yan ³, Li-Li Zhang ³, Gui-Jun Wan ⁴, Jun-Zheng Zhang ⁵ and Wei-Dong Pan ^{1,*}

¹ Beijing Key Laboratory of Bioelectromagnetics, Institute of Electrical Engineering, Chinese Academy of Sciences, Beijing, China

² University of Chinese Academy of Sciences, Beijing, China

³ Shanghai Synchrotron Radiation Facility, Shanghai Advanced Research Institute, Chinese Academy of Sciences, Shanghai, China

⁴ Department of Entomology, College of Plant Protection, Nanjing Agricultural University, Nanjing, China

⁵ Department of Plant Biosecurity and MOA Key Laboratory of Surveillance and Management for Plant Quarantine Pests, College of Plant Protection, China Agricultural University, Beijing, China

* Correspondence: panwd@mail.iee.ac.cn; Tel.: 86-10-82547168

Simple Summary

This study explored whether a hypomagnetic field, an environmental condition found in some places like deep space or shielded rooms, could worsen the problems associated with a genetic disease called Friedreich's ataxia. This disease is caused by a lack of a vital protein of frataxin that is essential for cellular iron–sulfur cluster biogenesis and oxidative balance. Using fruit flies as a model, researchers aimed to see if this hypomagnetic field would further disturb these elements and increase stress. They found that the hypomagnetic field changed iron and sulfur levels in very specific ways in different tissues, like the brain and eyes, and significantly increased harmful molecules in the brains of affected flies. It also altered the activity of genes related to iron and stress. The conclusion is that this environmental factor can indeed intensify the core cellular damage in this condition. This is valuable to society because it highlights how certain environmental conditions could potentially worsen symptoms for patients with similar metabolic diseases, informing future protective strategies.

Abstract

Frataxin is a conserved mitochondrial protein essential for cellular iron–sulfur (Fe–S) cluster biogenesis and oxidative balance, with its deficiency causing Friedreich's ataxia in humans. The hypomagnetic field (HMF), an environmental stressor known to influence oxidative stress and neurodevelopment, may interact with such inherent metabolic vulnerabilities. This study investigated whether HMF exposure exacerbates Fe–S homeostasis and oxidative disruption in a *Drosophila* model of frataxin deficiency. Using synchrotron radiation-based X-ray fluorescence (SR-XRF) spectroscopy for in-situ elemental analysis in live tissues, we found that HMF significantly altered iron distribution and content in a tissue-specific manner. In frataxin-silenced brains, HMF decreased iron distribution but increased total iron content, whereas in eyes it reduced iron content. Sulfur content decreased in frataxin-deficient eyes but increased in brains under HMF, though its spatial distribution was unchanged. Critically, HMF elevated reactive oxygen species (ROS) in frataxin-deficient brains. Transcriptomic analysis identified 202 differentially expressed genes under HMF in frataxin-silenced flies, including key regulators of iron metabolism and oxidative stress pathways. These findings demonstrate that HMF disrupts tissue-specific iron and sulfur homeostasis and intensifies oxidative stress in a frataxin-deficient insect system, underscoring its role as an environmental factor capable of aggravating metabolic fragility.

Keywords: hypomagnetic field; frataxin; SR-XRF; iron/sulfur; oxidative stress

1. Introduction

Frataxin, a nuclear-encoded mitochondrial protein, is universally recognized as a critical factor in iron-sulfur cluster (ISC) biogenesis and cellular iron homeostasis [1–6]. Its deficiency is the primary cause of Friedreich's ataxia (FRDA), a common hereditary neurodegenerative disease. Although its precise molecular functions are still being elucidated, a leading hypothesis posits that frataxin acts as an iron chaperone, serving as a finely-tuned "gatekeeper" that delivers ferrous iron to the scaffold protein ISCU and prevents premature or ineffective reactions during ISC assembly. Iron-sulfur clusters are vital cofactors for numerous metalloproteins involved in electron transport, enzymatic catalysis, and gene regulation. The consequences of frataxin deficiency are profound and conserved across model organisms, leading to mitochondrial iron accumulation, cytoplasmic iron depletion, reduced activity of Fe-S-dependent enzymes, and increased oxidative stress [7,8]. This cascade of mitochondrial dysfunction manifests clinically as impaired motor coordination, reduced lifespan, and, in the case of *Drosophila*, a specific developmental blockade [9,10].

The pathological cascade involved in frataxin deficiency is complex, culminating in late-stage mitochondrial iron accumulation. In *Drosophila* models, this iron directly drives neurodegeneration by activating the sphingolipid metabolism-Pdk1/Mef2 signaling axis—a pathway also conserved in mammalian hearts [11]. Given frataxin's established role in mitochondrial iron and redox metabolism, we propose investigating its function under environmental stressors that target these same pathways. One such stressor is the hypomagnetic field (HMF), a condition of significantly reduced magnetic flux relevant to deep-space exploration. As the geomagnetic field is thought to influence moving electric charges like electrons in the mitochondrial respiratory chain, we hypothesize that HMF exposure impairs mitochondrial function, potentially converging on pathways disrupted in FRDA. This is supported by preliminary observations of decreased motility under HMF, possibly due to reduced ATP production.

Given that iron dyshomeostasis is a pathological hallmark of FRDA [12]—initially revealed by granular iron deposits in cardiomyocytes—understanding the subcellular spatial distribution and chemical state of iron is critically important. To this end, we are leveraging the unique capabilities of synchrotron radiation-based X-ray fluorescence (SR-XRF) spectroscopy. The method of SR-XRF is ideally suited for acquiring quantitative, spatially resolved data on trace metal distributions and speciation with high resolution [13]. This study aims to use these insights to investigate the spatiotemporal dynamics of iron metabolism under the environmental stress of a hypomagnetic field, using *Drosophila melanogaster* as a model organism. We will employ microbeam XRF and to perform real-time, quantitative analysis of iron and sulfur content, distribution, and chemical states in live *Drosophila* tissues. Furthermore, in order to explore the differential gene expressions under hypomagnetic field exposure in frataxin-deficient flies, the comparative transcriptomes of frataxin-silenced and parental lines were sequenced using RNA-sequencing (RNA-Seq) technology and comparative analyses were performed to uncover the targeted alterations in genetic networks governing cellular oxidative stress responses and iron ion metabolism. Our goal is to elucidate the precise function and molecular pathways of frataxin in mediating these changes, thereby advancing our understanding of FRDA pathogenesis and opening avenues for new therapeutic interventions.

2. Materials and Methods

2.1. *Drosophila* Lines and Cultivation

The Gal4-UAS system was utilized for tissue-specific gene expression. The tub-Gal80^{ts}/CyO; repo-GAL4/TM6B lines obtained from China Agricultural University, were used to drive RNAi expression. The RNAi lines used in this work are as follows: UAS-*fh* RNAi (Bloomington Line Center,

BDSC 24620). *Drosophila* stocks were cultivated at $25 \pm 1^\circ\text{C}$, with relative humidity $60\% \pm 5\%$ and 12:12 h light: dark cycle. All magnetic field exposure assays were performed at 25°C . For genotypes carrying tub-GAL80^{ts} (repo-GAL4; tub-GAL80^{ts} > *fh*-RNAi), flies were reared at 18°C during development and shifted to 29°C at 3–5 days post-eclosion to induce adult-onset RNAi, followed by magnetic field exposure at 25°C . In contrast, the *ninaE*-GAL4 > *fh*-RNAi flies (without tub-GAL80^{ts}) were maintained at 25°C throughout the whole experiments. Standard regular diet (RD): agar 20 g/L, sucrose 80 g/L, active dry yeast 5 g/L, calcium chloride dihydrate 1.6 g/L, ferrous sulfate heptahydrate 1.6 g/L, sodium potassium tartrate tetrahydrate 8 g/L, sodium chloride 0.5 g/L, manganese chloride tetrahydrate 0.5 g/L, and nipagin 5.3 mL/L [14].

2.2. Construction of Frataxin-Silenced *Drosophila* Mutants Using RNAi

The GAL4/UAS system employed to generate frataxin gene silencing in different tissues. The *Drosophila* lines were maintained on a cornmeal-agar medium at 25°C . To achieve time-controlled silencing of frataxin (*fh*) in glial cells (repo-GAL4; tub-GAL80^{ts} > *fh*-RNAi), we employed the GAL4/UAS system combined with tub-GAL80^{ts}. In addition, to silence *fh* specifically in retinal photoreceptors, we used *ninaE*-GAL4 > *fh*-RNAi (without GAL80^{ts}) as a retina-specific (non-time-controlled) knockdown strategy. The genetic control was one of the parental lines, UAS-*fh* RNAi. Virgin female flies from one of the parental lines were selected for hybridization. Hybridization experiments were conducted to generate F1 generations with silenced frataxin in glial cells (repo-GAL4; tub-GAL80^{ts} > *fh*-RNAi) and retinal cells (*ninaE*-GAL4 > *fh*-RNAi) (Figure 1). For all crosses involving GAL80^{ts}, both parents and their developmental-stage offspring were reared at 18°C to suppress GAL4 activity. To induce target gene silencing, F1 offspring were transferred to 29°C post-eclosion. Upon reaching adulthood, F1 individuals were sorted for specific phenotypes to establish the silencing model.

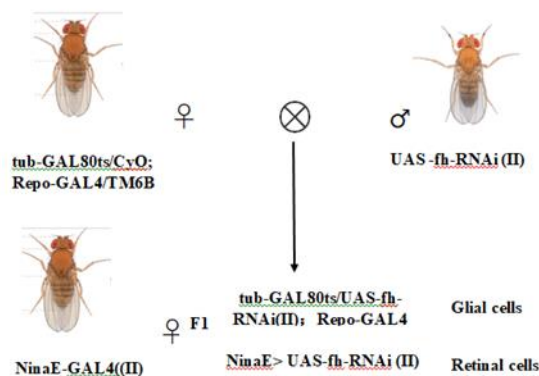


Figure 1. *Drosophila* mutants with frataxin silencing in glial and retinal cells.

2.3. Magnetic Field Generation System and Insect Exposures

The experiment was conducted in a laboratory in Beijing ($39^\circ 59' 14''\text{N}$, $116^\circ 19' 21''\text{E}$), where the local geomagnetic field (GMF) has an intensity of $52,487 \pm 841$ nT, a declination of $5.30 \pm 0.59^\circ$, and an inclination of $56^\circ 29' \pm 1.02^\circ$. To create a hypomagnetic field (HMF), we employed three sets of Helmholtz coils, each powered independently to generate an artificial field that precisely opposed and offset each vector component of the local GMF for nullifying the total intensity of GMF. This setup produced a spherical hypomagnetic environment of $300 \times 300 \times 300$ mm³ with an average residual intensity <500 nT (Figure 2). The external diameter of HMF system is 1200 mm, and insects are placed on the wooden table in middle of Helmholtz coils during experiments. A fluxgate magnetometer (Honor Top model 191A, sensitivity ± 1 nT) was used to calibrate and verify the HMF intensity twice daily, both before and after experimental sessions.

The *Drosophila* flies used for the HMF exposure were 3-10 days-old adult flies, from *fh*-RNAi flies. The flies were housed in groups of 20 per tube, with three replicate groups per condition. Each experimental cycle consisted of a 72-hour exposure to either the HMF or the normal GMF, under a light-dark regimen of 12 hours of light followed by 12 hours of darkness.

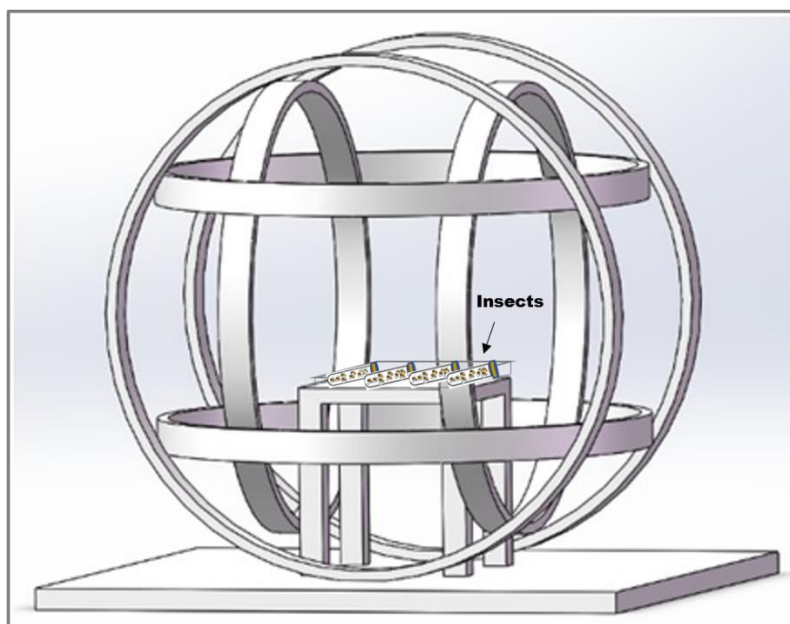


Figure 2. The Helmholtz coil system used to generate hypomagnetic fields (HMF). The system consists of three independent coil pairs and each pair of coils are individually powered. The external diameter of apparatus is 1200 mm. The effective area of HMF is generated in the center space with 300×300×300 mm³. Insects are placed on the wooden table in middle of Helmholtz coils.

2.4. Synchrotron Radiation-Based X-Ray Fluorescence (SR-XRF) and Elemental Distribution & Quantitative Measurements of Iron/Sulfur in Glial and Retinal Cells

To investigate the composition and spatial distribution of iron & sulfur within the microregions of living tissues, brain and eye tissues from *Drosophila* flies exposed to either HMF or GMF conditions were analyzed using microbeam X-ray fluorescence (μ -XRF). The experiments were conducted at the wiggler beamlines 6-2, 10-2 at BL15U1 of the Shanghai Synchrotron Radiation Facility (SSRF) (Shanghai, China). The BL15U1 beamline enables multi-element mapping and quantitative analysis at the sub-parts per million level, utilizing a micron or sub-micron beam. During analysis, the sample was oriented at a 45° angle to the incident X-ray beam, while the X-ray Vortex-90EX Silicon drift detector (SDD), is perpendicular to the beam incidence. The ion chamber is used to monitor the incident photon intensity. An integrated optical microscope facilitated sample observation. The μ -XRF scanning was performed in stepwise mode, with the spectrum for each pixel saved for subsequent quantitative analysis. For data analysis, the software packages GeoPIXE and PyMCA were employed [15–17]. Regions of interest (ROIs) on the spectra can be selected. Once ROIs are created, they are applied across all collected data points to generate two-dimensional, multi-element maps visualizing the distribution of the target elements.

2.5. ROS Detection Using DHE Staining and Confocal Microscopy

A 2 mM solution of dihydroethium (DHE) was prepared using DMSO as the solvent. 500 μ L of PBS buffer was combined with 2 μ L of DHE stock (2 mM) to achieve a final working concentration of 8 μ M. *Drosophila* flies of the appropriate genotype and age were selected and transferred using tweezers to a glass 9-well plate containing PBS for dissection under a stereomicroscope. The dissected brain and eye tissues were then placed into a 96-well plate containing DHE solution. DHE solution

was removed, and the samples were washed twice with fresh PBS buffer. Subsequently, 200 μ L of 4% PFA solution was added for fixation at room temperature for 5 minutes. Following suctioning of the fixative, the samples were washed twice with PBS before secondary dissection, film sealing and imaging were performed. Five biological replicates were conducted for each treatment.

At least 5-10 flies per genotype were scanned. The samples were analyzed using a LSM 510 Confocal Microscope (Zeiss, Germany). All images were acquired using the same exposure, light intensity and filter settings for all conditions. Confocal images were further processed with the image processing software Fiji 2.0.0 [18] and contrast of each image was adjusted to improve quality of signal.

2.6. RNA-Seq and Differential Gene Expression Analysis

Total RNA was extracted from heads of 3-8 days-old adult flies. For each genotype, three biological replicates with five heads of flies for each replicate were sent to Novogene for RNA-Seq analysis using TRNzol Universal Reagent (Cat. No. DP424) according to the manufacturer's instructions. RNA quantity and integrity were verified on a Nanodrop 2000 (Thermo) and only high-quality RNA was used for library preparation. Sequencing libraries were constructed with the Fast RNA-seq Lib Prep Kit V2 (Cat. No. RK20306) following the supplier's protocol. The clean reads were aligned to the corresponding reference genome using HISAT2 (v2.2.1). Read counts for each gene were obtained with feature Counts (v2.0.6), and gene expression levels were estimated as fragments per kilobase of transcript per million mapped reads (FPKM). Differentially expressed genes (DEGs) between groups were identified using the R package DESeq2 (v1.42.0), with Benjamini-Hochberg correction to control the false discovery rate. Genes with adjusted P value (padj) ≤ 0.05 and $|\log_2(\text{fold change})| \geq 1$ were considered significantly differentially expressed. Functional enrichment analyses of DEGs were performed using cluster Profiler (v4.8.1) for Gene Ontology (GO) and KEGG pathway enrichment. Gene set enrichment analysis (GSEA) was conducted with the GSEA software (v4.3.2) using default parameters and curated GO/KEGG gene sets.

2.7. Statistics

Data analysis was performed using the SPSS version 23.0 software (IBM SPSS Statistics Inc., Chicago, USA). First, a uniform intensity threshold was set based on the background signal of the element distribution map. The number of pixels above this threshold was counted and used as a quantitative indicator of the relative distribution of corresponding elements (iron, sulfur) in brain and eye tissues. Based on this, normality and homogeneity of variance tests were performed for iron & sulfur content and distribution counts, respectively. When parametric tests were feasible, one-way ANOVA followed by Tukey's post hoc multiple comparisons were conducted. The effects of magnetic field conditions and genotypes as independent variables to evaluate the effects of different magnetic fields and genotypes on element content and distribution in brain and eye tissues. The Shapiro-Wilk test was used to test the normality of the data. The data conforming to the normal distribution were expressed as mean \pm SEM (standard error of the mean). An outlier would be dropped if it was observed due to incorrect entry or measurement of the data. The independent-samples t-test was performed to evaluate effects of different magnetic fields and genotypes on ROS level in brain and eye tissues. One-way repeated-measures ANOVA with Tukey's post-hoc test was used for the effects of frataxin gene silencing on the distribution and content of iron/sulfur in brain or eye tissues of *Drosophila melanogaster* under GMF or HMF. Fisher's least significant difference method was utilized to examine differences between groups. P values < 0.05 were considered statistically significant.

3. Results

3.1. Analysis of Iron/Sulfur Elemental Distribution and Content Based on Frataxin Silencing Model Under GMF or HMF

3.1.1. Iron Elemental Analysis

Compared with the control group, the frataxin-silenced group, either in brain or eye tissues, showed no significant difference in iron elemental distribution ($P>0.05$) and fluorescence area ($P>0.05$) under GMF exposure (Figure 3). However, in brain tissues, iron elemental distribution was significantly decreased ($P<0.05$) in frataxin-silenced flies within HMF exposure, while no significant difference was shown in either fluorescence area ($P>0.05$) or total fluorescence intensity ($P>0.05$) in frataxin-silenced group (Figure 3). Moreover, in eye tissues, neither significant difference in iron elemental distribution ($P>0.05$) or in fluorescence area ($P>0.05$) in frataxin-silenced flies was revealed between GMF and HMF exposure (Figure 3).

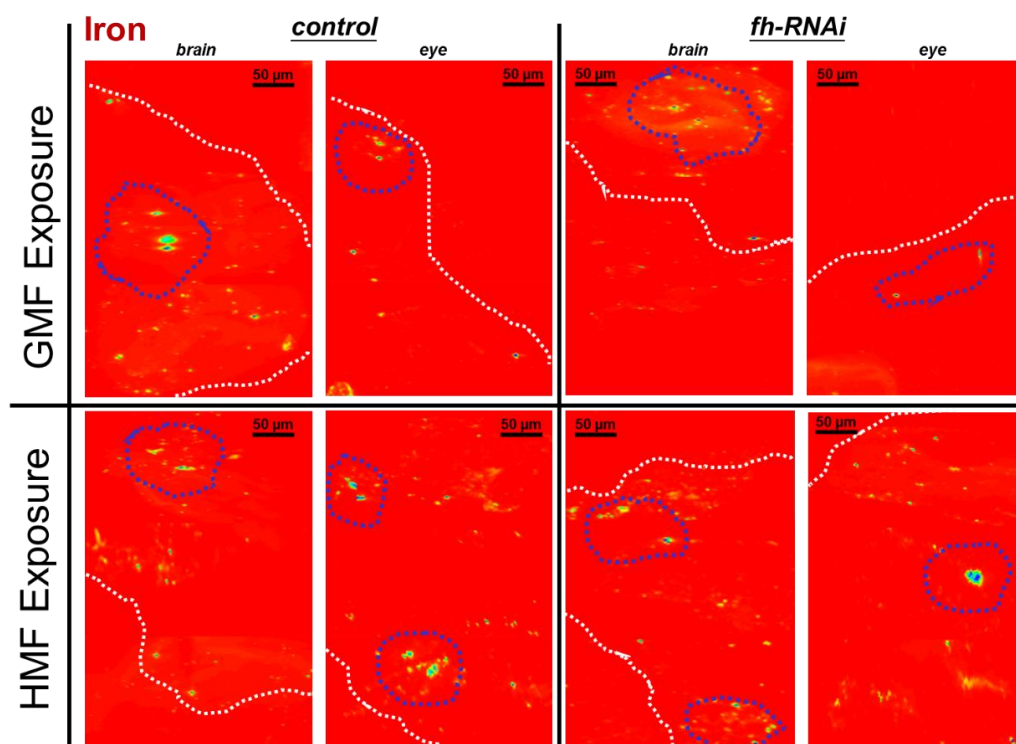


Figure 3. Iron elemental distribution in brain and eye tissues of *Drosophila melanogaster* within GMF or HMF exposure. The genetic control was UAS-*fh* RNAi and frataxin silencing in brain and eye tissues were lines of *repo-GAL4; tub-GAL80^{ts}>fh-RNAi* and *ninaE-GAL4> fh-RNAi*, respectively. Pixel size in the images is 2 µm; scan time is 50 ms. Elemental maps were measured in “2D F1Y Scan” mode and normalized to dead time. Red striped circles indicate areas with iron hot-spots, and white striped lines arrow the range of scanned iron.

Compared with the control group, the iron content in brain and eye tissues after frataxin silencing decreased by 35.73% ($P<0.05$) and 16.51% ($P<0.05$), respectively (Figure 4A). Compared with GMF, the iron content in brain tissues of frataxin-silenced flies increased by 46.71% ($P<0.05$), while that in eye tissues after frataxin silencing decreased by 24.57% ($P<0.05$) under HMF exposure (Figure 4B).

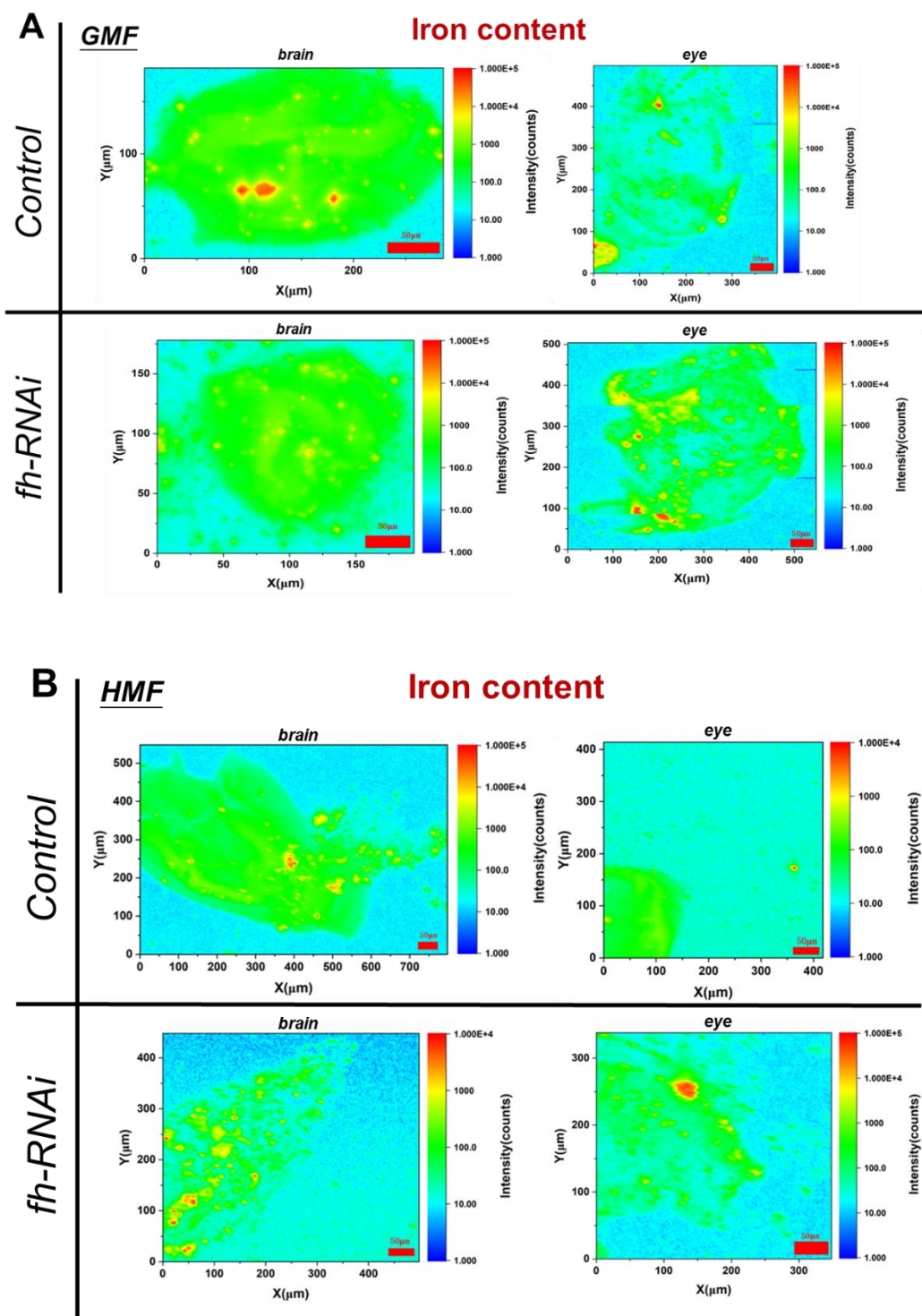


Figure 4. Iron content in brain (A) and eye (B) tissues of *Drosophila melanogaster* within GMF or HMF exposure. The genetic control was UAS-*fh* RNAi and frataxin silencing in brain and eye tissues were lines of repo-GAL4; tub-GAL80^{ts}> *fh*-RNAi and ninaE-GAL4> *fh*-RNAi, respectively. Scale bar indicates the background-corrected intensity of scanned iron in counts.

3.1.2. Sulfur Elemental Analysis

Compared with the control group, frataxin-silenced group showed no significant difference in sulfur elemental distribution in brain or eye tissues ($P>0.05$), as well as showed no significant difference in fluorescence area in either of both tissues ($P>0.05$). Compared with GMF exposure,

frataxin silencing either in brain or eye tissues showed no significant difference in sulfur elemental distribution ($P>0.05$) or fluorescence area ($P>0.05$) under HMF exposure (Figure 5).

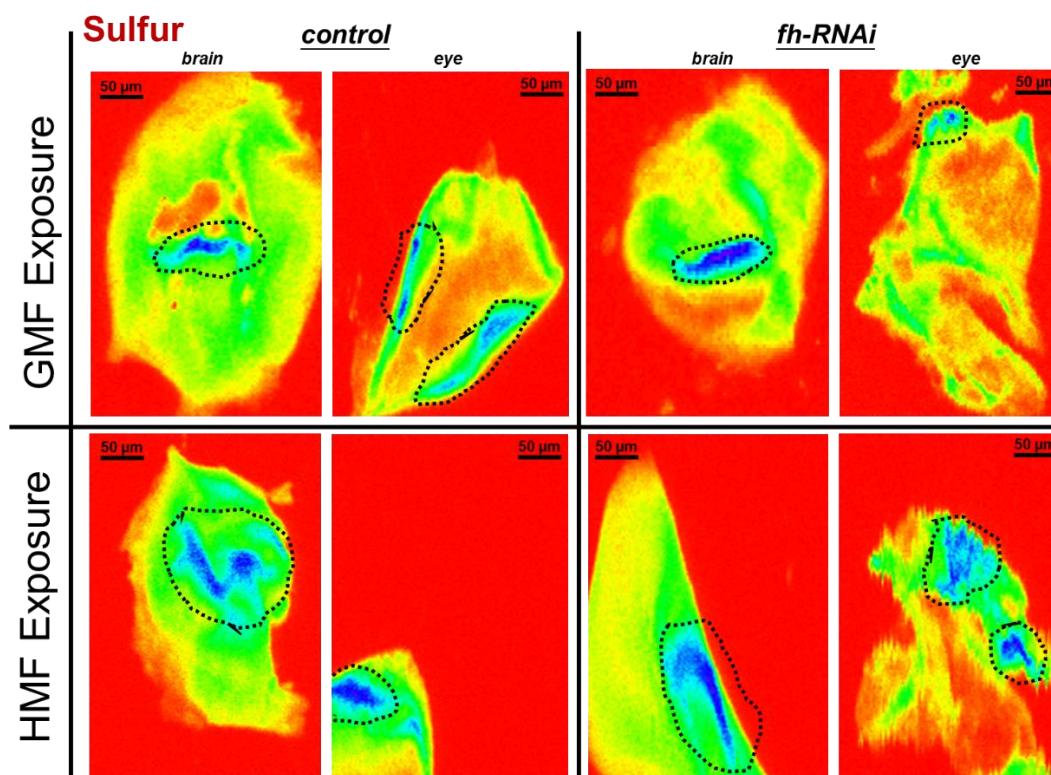


Figure 5. Sulfur elemental distribution in brain and eye tissues of *Drosophila melanogaster* within GMF or HMF exposure. The genetic control was UAS-*fh* RNAi and frataxin silencing in brain and eye tissues were lines of *repo-GAL4; tub-GAL80^{ts}> fh-RNAi* and *ninaE-GAL4> fh-RNAi*, respectively. Pixel size in the images is 2 μm ; scan time is 50 ms. Black striped circles indicate areas with sulfur hot-spots (blue ROIs).

Compared with the control group, the sulfur content in eye tissues after frataxin silencing decreased by 18.76% ($P<0.05$), and no significance in the sulfur content in brain tissues was observed with frataxin-silenced group ($P>0.05$) (Figure 6A). Compared with GMF exposure, the sulfur content in brain tissues after frataxin silencing was reduced by 40.48% ($P<0.05$) and that in eye tissues with frataxin-silenced group elevated by 65.05% ($P<0.05$) within HMF exposure (Figure 6B).

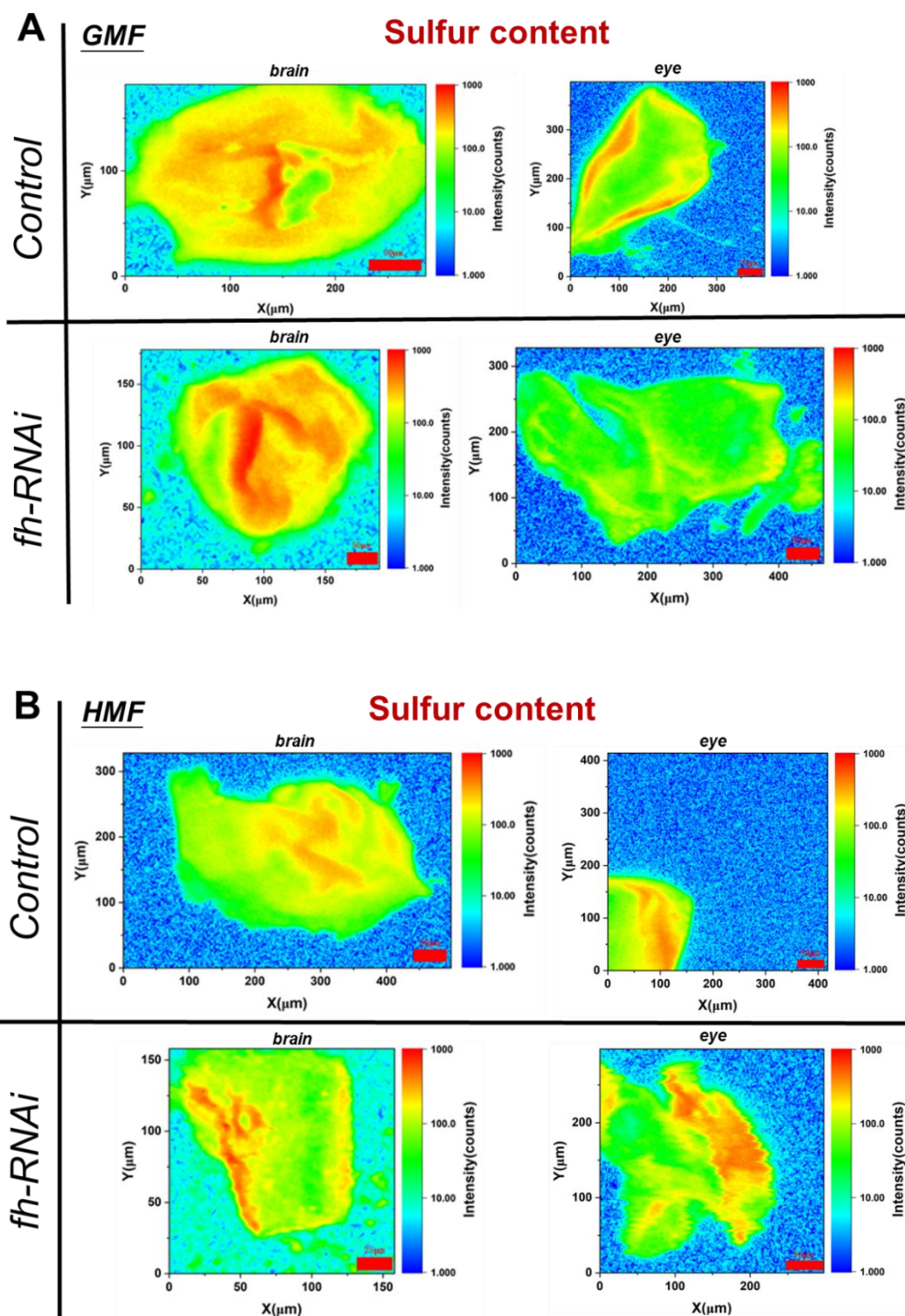


Figure 6. Sulfur content in brain (A) and eye (B) tissues of *Drosophila melanogaster* within GMF or HMF exposure. The genetic control was UAS-*fh* RNAi and frataxin silencing in brain and eye tissues were lines of repo-GAL4; tub-GAL80^{ts} > *fh*-RNAi and ninaE-GAL4 > *fh*-RNAi, respectively. Scale bar indicates the background-corrected intensity of scanned sulfur in counts.

3.2. ROS Detection Using DHE Staining

DHE is a lipophilic, cell-permeable probe that is itself non-fluorescent. Upon oxidation by cellular reactive oxygen species (ROS)—primarily superoxide—it is converted to ethidium. Ethidium then binds to DNA, producing a red fluorescence (excitation/emission 520/610 nm) that serves as an

indicator of intracellular ROS levels. For samples stained with DHE, the mean fluorescence intensity provides a more appropriate measurement of ROS levels.

As shown in brain tissues (Figures 7 and 8), no significant difference in ROS levels were discovered between GMF control and HMF control group ($P>0.05$). However, compared with GMF exposure, ROS levels were significantly elevated in frataxin-silenced brain samples under HMF conditions ($P<0.001$; Figure 8). Corresponding confocal images showed this rise as more intense red fluorescence was observed (Figure 5). In contrast to brain samples, it was found that in eye tissues, compared with GMF exposure, ROS levels revealed no significant difference either with control group ($P>0.05$) or with frataxin-silenced group under HMF exposure ($P>0.05$) (Figure 8), which were further confirmed by corresponding confocal microscopy (Figure 7).

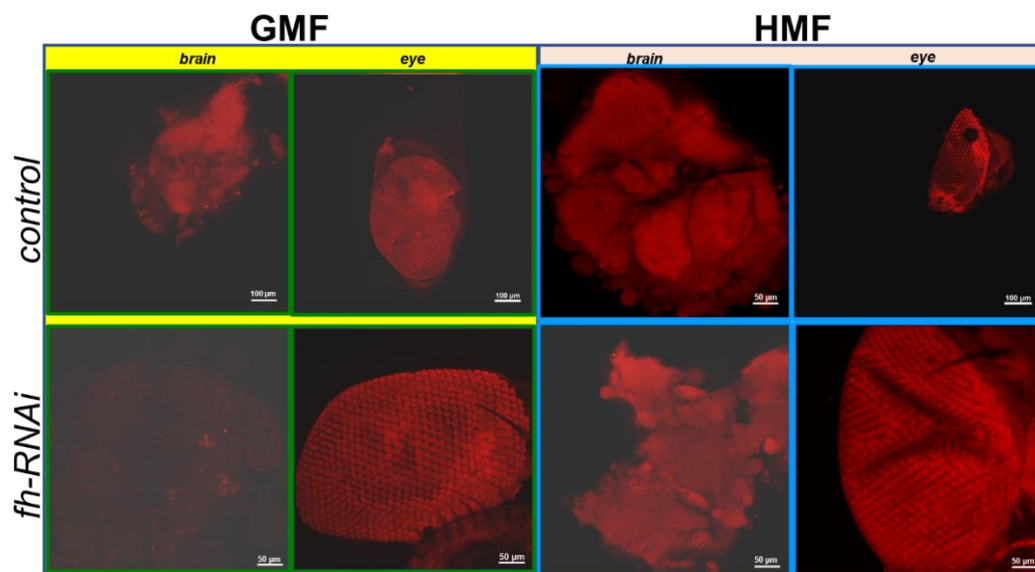


Figure 7. ROS examination of brain and eye tissues of *Drosophila melanogaster* using laser scanning confocal immunofluorescence with dihydroethidium staining. Intracellular ROS levels were visualized as a red fluorescence excited from oxidized ethidium. The mean fluorescence intensity serves as an indicator of ROS levels. The genetic control was UAS-*fh* RNAi and frataxin silencing in brain and eye tissues were lines of repo-GAL4; tub-GAL80^{ts}> *fh*-RNAi and *ninaE*-GAL4> *fh*-RNAi, respectively.

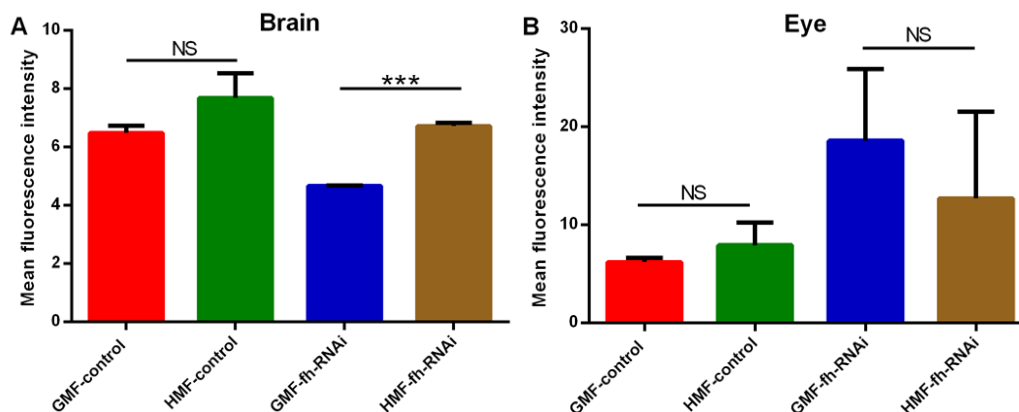


Figure 8. ROS levels of brain and eye tissues of *Drosophila melanogaster* as indicated by mean fluorescence intensity. The genetic control was UAS-*fh* RNAi and frataxin silencing in brain and eye tissues were lines of repo-GAL4; tub-GAL80^{ts}> *fh*-RNAi and *ninaE*-GAL4> *fh*-RNAi, respectively. The independent-samples t-test ($***P<0.001$; NS, not significant) was performed to evaluate effects of different magnetic fields or genotypes on ROS level in brain and eye tissues. Data are presented as the means \pm SEM.

3.3. Analysis of DEGs with HMF Exposure Specifically in Iron Metabolism, ROS Production and Antioxidation

A comparison of frataxin-silenced and control flies under HMF exposure identified a total of 202 differentially expressed genes (DEGs), confirming frataxin's substantial role in gene regulation. Similarly, 252 DEGs were found under GMF exposure (Figure 9). It was noted that the influence of the magnetic environment itself was underscored by 260 DEGs between the two frataxin-silenced groups (GMF fh-RNAi vs HMF fh-RNAi) and 329 DEGs between the two control groups (Figure 9), highlighting that hypomagnetic fields significantly enhance transcriptional profiles of tissues in *Drosophila* flies.

Exposure to HMF prompted remodeling of pathways related to iron metabolism and oxidative stress. In the control group, key DEGs involved in iron metabolic regulation, such as cytochrome P450 molecules (6w1/304a1/6d2), were upregulated. ROS sources including NADPH oxidase and quiescin sulfhydryl oxidase were also increased, alongside activation of antioxidants like glutathione S-transferase, superoxide dismutase, and peroxidase (Table 1). In contrast, the frataxin-silenced group under HMF showed downregulation of DEGs encoding heme-binding (CG5157) and ferroxidase activities (multicopper oxidase 1/3), as well as reduced ROS-producing enzymes (NADPH oxidase and dual oxidase) (Table 2). Despite the downregulation of peroxiredoxin, antioxidants such as glutathione S-transferase and catalase were upregulated, suggesting a compensatory protective response alike to that of the control group (Table 2).

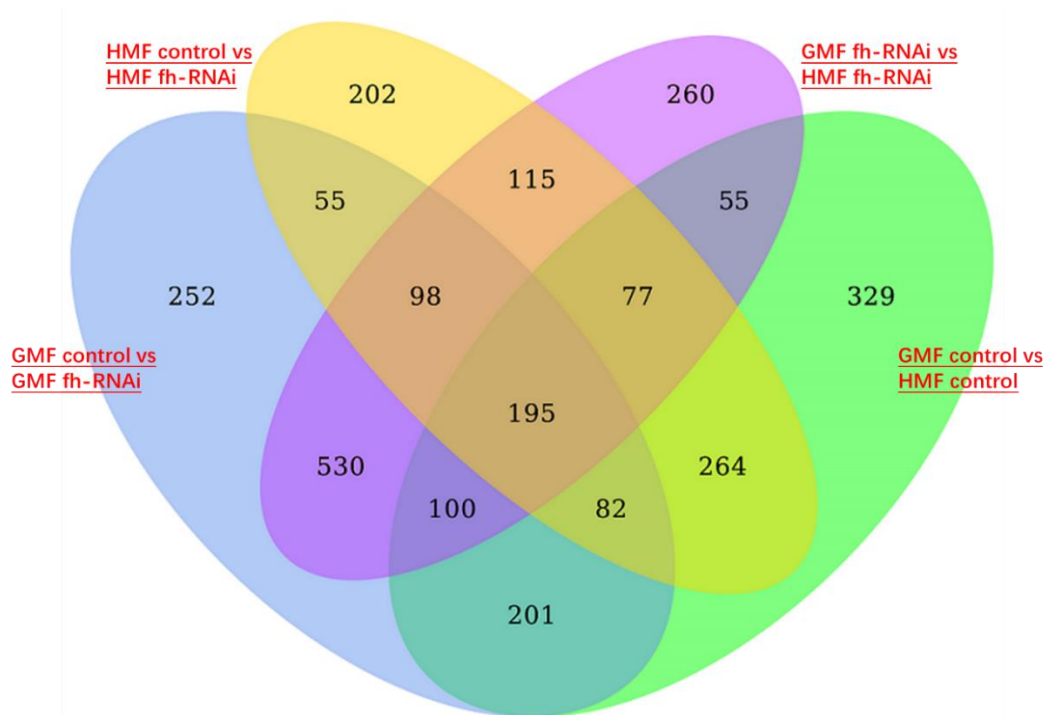


Figure 9. Venn diagram showing four lists of differentially expressed genes in heads of frataxin-silenced flies and in flies exposed to hypomagnetic fields. The genetic control was UAS-*fh* RNAi and frataxin silencing in brain tissues of heads was line of repo-GAL4; tub-GAL80^{ts}>*fh*-RNAi.

Table 1. Selected differentially expressed genes (DEGs) that are involved in iron metabolism, ROS production and antioxidation in heads of UAS-*fh* RNAi (control) flies after HMF exposure.

Gene_ID	log ₂ FoldChange	pval	padj	Gene_description
FBgn0033065	2.418363708	0	0	Cytochrome P450 6w1 (Iron metabolism)
FBgn0038095	4.877657598	9.40E-200	1.10E-197	Cytochrome P450 304a1 (Iron metabolism)
FBgn0034756	3.355233071	2.80E-128	2.05E-126	Cytochrome P450 6d2 (Iron metabolism)
FBgn0085428	1.023945	6.22E-07	2.93E-06	NADPH oxidase (ROS production)

FBgn0038919	1.03	2.40E-07	1.19E-06	Quiescin sulfhydryl oxidase 2 (ROS production)
FBgn0010041	2.773212	8.10E-10	4.92E-09	Glutathione S-transferase D5 (Antioxidation)
FBgn0010040	2.7611	5.87E-05	0.0002194	Glutathione S-transferase D4 (Antioxidation)
FBgn0051028	1.682223	1.37E-07	6.91E-07	Related to SOD (Antioxidation)
FBgn0004577	3.186946	4.77E-05	0.0001803	Peroxidase (Antioxidation)

Criteria for differentially expressed genes: $|\log_2(\text{FoldChange})| > 1$ & $\text{padj} < 0.05$.

Table 2. Selected differentially expressed genes (DEGs) that are involved in iron metabolism, ROS production and antioxidation in heads of *repo-GAL4; tub-GAL80^{ts} fh-RNAi (fh-RNAi)* flies after HMF exposure.

Gene_ID	log ₂ FoldChange	pval	padj	Gene_description
FBgn0036575	-2.6845	2.45E-07	1.18E-06	CG5157 (Iron metabolism)
FBgn0032116	-1.89932	1.27E-104	6.46E-103	Multicopper oxidase 1 (Iron metabolism)
FBgn0039387	-3.35859	1.75E-07	8.53E-07	Multicopper oxidase 3 (Iron metabolism)
FBgn0085428	-1.92347	3.01E-18	2.88E-17	NADPH oxidase (ROS production)
FBgn0283531	-1.18372	2.70E-31	4.12E-30	Dual oxidase (ROS production)
FBgn0033520	-1.3659	0.0003142	0.0010317	Peroxiredoxin 6b (Antioxidation)
FBgn0010041	1.988693	9.08E-11	5.71E-10	Glutathione S transferase D5 (Antioxidation)
FBgn0010042	2.880674	5.37E-05	0.0001985	Glutathione S transferase D6 (Antioxidation)
FBgn0038465	1.271917	5.63E-307	1.22E-304	Immune-regulated catalase (Antioxidation)

Criteria for differentially expressed genes: $|\log_2(\text{FoldChange})| > 1$ & $\text{padj} < 0.05$.

4. Discussion

In *Drosophila*, frataxin is suggested to maintain mitochondrial Fe-S cluster synthesis and iron metabolic homeostasis, and its deficiency leads to impaired energy metabolism, oxidative stress, and neurodegenerative phenotypes [7,8,19–23]. The discovery of iron deposits in the hearts of FRDA patients in the late seventies [24,25] was the first indication of an association between frataxin and this transition metal, and increased iron content has been reported in critical brain areas of FRDA patients [26,27]. In *Drosophila*, Chen et al. showed that iron accumulates in the nervous system in *fh*¹ mutants [11]. In this study, the role of frataxin in iron metabolism and oxidative stress under environmental stressor such as hypomagnetic field was investigated primarily using SR-XRF spectroscopy. After frataxin silencing, no significant change either in iron/sulfur elemental distribution or fluorescence area was revealed (Figures 3 and 5). After HMF exposure, however, significant changes happened in iron elemental distribution in frataxin-silenced brain tissues. Moreover, after frataxin silencing, the iron content in both target tissues decreased (Figure 4A), while the iron content in brain and eye tissues of frataxin-silenced flies increased and decreased under HMF exposure, respectively (Figure 4B). The sulfur content showed similar trend of changes within frataxin silencing (Figure 5A), except the opposite trend of changes in sulfur content in frataxin-silenced tissues after HMF exposure (Figure 6B). These findings suggested that while iron plays an instrumental role in *Drosophila* frataxin biology, HMF may impose more crucial impact on the iron/sulfur homeostasis, owing to more delicate techniques to dissect the spatiotemporal dynamics of this process in a living model organism.

The knockdown or mutation of *Drosophila* frataxin (*d_{fh}*) leads to decreased activity of Fe-S-dependent enzymes (e.g., cis-aconitase, complexes I-III), and also leads to iron metabolic variations and elevated ROS, especially in neural and muscular tissues [28–30]. In *Drosophila*, using the *fh*-RNAi line and the actin GAL4-driver line [31,32], the flies with tissue-specific frataxin deficiency in the PNS (C96) or glial cells (repo) showed increased sensitivity to external oxidative stressors such as hyperoxia or H₂O₂ treatment [23,31,33]. However, the ROS hypothesis has been questioned in several studies, reporting that loss of FXN leads to a hypersensitivity to ROS, rather than elevated ROS levels [1,8,28,34,35]. In our study, although significant change of ROS levels in brain tissues of control group was not determined under HMF exposure, elevated ROS levels were discovered in frataxin-silenced group within HMF conditions (Figures 7 and 8). Combined these data suggest that ROS appears more to be a tissue-specific “provider of feedback” for HMF rather than a prominent player in model organisms.

A large amount of DEGs between frataxin-silenced and control flies under either GMF or HMF exposure demonstrated frataxin's crucial role in gene regulation in terms of iron metabolism and oxidative stress. To our interests, more DEGs were revealed using HMF as treatment, amongst them key DEGs involved in iron metabolic regulation, ROS source, and antioxidant were activated, suggesting the synergistic effect of ROS source for HMF with the iron metabolic homeostasis via frataxin associated traits in *Drosophila* flies.

The proposed methodology of using SR-XRF spectroscopy on live *Drosophila* tissues is a standout feature and improvement over traditional approaches. The ability to perform real-time, quantitative analysis of both iron/sulfur content and distribution at a mutant/parent-type level in a living organism is powerful in this context [17]. This approach promises to move beyond snapshots and provide a “movie” of metabolic alterations, directly testing the gatekeeper hypothesis by observing how the absence of frataxin disrupts the precise choreography of iron and sulfur under stress conditions.

Moreover, we used pan-glial driver repo-GAL4 instead of pan-neuronal driver elav-GAL4 to achieve targeted frataxin knockdown because the repo-GAL4 is widely expressed in glial cells, allowing us to simulate frataxin deficiency in nervous system related tissues while avoiding systemic knockout that could lead to severe developmental defects or fatal outcomes from elav-GAL4-driven neuronal knockdown [36]. As elav-GAL4 drives broad expression early in nervous system development, and *fh* is a core mitochondrial gene, widespread neuronal impairment during development may alter circuit formation, baseline activity, feeding, and developmental rate. In addition, tissue-specific knockdown reduces the risk of developmental mortality that may result from general silencing. Nevertheless, pan-neuronal knockdown could be informative and will be addressed in future work to dissect cell-type contribution.

5. Conclusions

In conclusion, our study demonstrates that the hypomagnetic field acts as a significant environmental stressor, capable of exacerbating the inherent metabolic fragility in a frataxin-deficient insect system. By disrupting tissue-specific homeostasis of iron & sulfur, elevating reactive oxygen species, and altering the expression of key metabolic genes, HMF exposure aggravates the pathological processes linked to Friedreich’s ataxia. These findings underscore the potential role of environmental magnetic fields in influencing the progression of genetic metabolic disorders. By combining a robust insect model with state-of-the-art, real-time SR-based X-ray fluorescence, this study is also poised to provide more profound insights into the function of frataxin, the cascade of events following its deficiency, and potentially pursue new targets for therapeutic intervention.

Author Contributions: Conceptualization, Weidong Pan and Huiming Kang; methodology, Huiming Kang, Shuai Yan and Lili Zhang ; formal analysis, Huiming Kang and Shuai Yan; investigation, Huiming Kang; resources, Shuai Yan and Junzheng Zhang; data curation, Huiming Kang and Junzheng Zhang; writing—original draft preparation, Huiming Kang and Weidong Pan; writing—review and editing, Weidong Pan and

Guijun Wan; supervision, Weidong Pan and Junzheng Zhang; project administration, Weidong Pan; funding acquisition, Weidong Pan, Guijun Wan and Shuai Lili Zhang. All authors have read and agreed to the published version of the manuscript.

Funding: This research was supported by the National Natural Science Foundation of China (32271286, 32172414), the National Key Research and Development Program of China (SQ2023YFA1600106), and the Natural Science Foundation of Jiangsu Province (BK20221510).

Data Availability Statement: The authors confirm that the data supporting the findings of this study are available within the article.

Acknowledgments: We thank our technical group for their assistance in keeping insect stocks and maintaining the exposure equipment.

Conflicts of Interest: The authors declare no conflicts of interest. The funders had no role in the design of the study; in the collection, analyses, or interpretation of data; in the writing of the manuscript; or in the decision to publish the results.

Abbreviations.

The following abbreviations are used in this manuscript:

<i>fh</i>	Frataxin
SR-XRF	Synchrotron radiation-based X-ray fluorescence
UAS	Upstream activating sequence
GMF	Geomagnetic field
HMF	Hypomagnetic field

References

1. Babcock, M.; de Silva, D.; Oaks, R.; Davis-Kaplan, S.; Jiralerspong, S.; Montermini, L.; Pandolfo, M.; Kaplan, J. Regulation of mitochondrial iron accumulation by Yfh1p, a putative homolog of frataxin. *Science*, 1997, 276, 1709–1712.
2. Schmucker, S.; Martelli, A.; Colin, F.; Page, A.; Wattenhofer-Donzé, M.; Reutenauer, L.; *et al.* Mammalian frataxin: An essential function for cellular viability through an interaction with a preformed ISCU/NFS1/ISD11 iron-sulfur assembly complex. *PLoS ONE*, 2011, 6, e16199.
3. Vaubel, R.A.; Isaya, G. Iron-sulfur cluster synthesis, iron homeostasis and oxidative stress in Friedreich ataxia. *Molecular and Cellular Neuroscience*, 2013, 55, 50-61.
4. Maio, N.; Jain, A.; Rouault, T.A. Mammalian iron–sulfur cluster biogenesis: Recent insights into the roles of frataxin, acyl carrier protein and ATPase-mediated transfer to recipient proteins. *Current Opinion in Chemical Biology*, 2020, 55, 34-44.
5. Campbell, C.J.; Pall, A.E.; Naik, A.R.; Thompson, L.N.; Stemmler, T.L. Molecular details of the frataxin–scaffold interaction during mitochondrial Fe–S cluster assembly. *International Journal of Molecular Sciences*, 2021, 22, 6006.
6. Anderson, P.R.; Kim, K.; Hilliker, A.J.; Phillips, J.P. RNAi-mediated suppression of the mitochondrial iron chaperone, frataxin, in *Drosophila*. *Human Molecular Genetics*, 2005, 14(22), 3397-3405.
7. Llorens, J.V.; Navarro, J.A.; Martínez-Sebastián, M.J.; Baylies, M.K.; Schneuwly, S.; Botella, J.A.; *et al.* Causative role of oxidative stress in a *Drosophila* model of Friedreich ataxia. *FASEB Journal*, 2007, 21, 333-344.
8. Amandine, P.; David, L.; Joëlle, C.T.; Hervé, T.; Véronique, M. Frataxin inactivation leads to steroid deficiency in flies and human ovarian cells. *Human Molecular Genetics*, 2015, 24, 2615-2626.
9. Rawat, S.; Kondapalli, K.C.; Rodrigues, A.V.; Stemmler, T.L. Backbone resonance assignments and secondary structure of the apo-*Drosophila melanogaster* frataxin homolog (*dfh*). *Biomolecular NMR Assignments*, 2019, 13, 377-381.

10. Chen, K.; Ho, T.S.Y.; Lin, G.; Tan, K.L.; Rasband, M.N.; Bellen, H.J. Loss of frataxin activates the iron/sphingolipid/PDK1/Mef2 pathway in mammals. *eLife*, 2016, 5, e20732.
11. Bradley, J.L.; Blake, J.C.; Chamberlain, S.; Thomas, P.K.; Cooper, J.M.; Schapira, A.H.V. Clinical, biochemical and molecular genetic correlations in Friedreich's ataxia. *Human Molecular Genetics*, 2000, 9(2), 275-282.
12. De Samber, B.; Meul, E.; Laforce, B.; De Paepe, B.; Smet, J.; De Bruyne, M.; *et al.* Nanoscopic X-ray fluorescence imaging and quantification of intracellular key-elements in cryofrozen Friedreich's ataxia fibroblasts. *PLoS ONE*, 2018, 13, e0190495.
13. Villanueva, J.E.; Liveló, C.; Trujillo, A.S.; Chandran, S.; Woodworth, B.; Andrade, L.; *et al.* Time-restricted feeding restores muscle function in *Drosophila* models of obesity and circadian-rhythm disruption. *Nature Communications*, 2019, 10, 2700.
14. Ryan, C.G.; Cousens, D.R.; Sie, S.H.; Griffin, W.L. Quantitative analysis of PIXE spectra in geoscience applications. *Nuclear Instruments and Methods in Physics Research Section B: Beam Interactions with Materials and Atoms*, 1990, 49, 271-276.
15. Solé, V.A.; Papillon, E.; Cotte, M.; Walter, P.; Susini, J. A multiplatform code for the analysis of energy-dispersive X-ray fluorescence spectra. *Spectrochimica Acta Part B: Atomic Spectroscopy*, 2007, 62, 63-68.
16. Zhang, L.; Yan, S.; Jiang, S.; Yang, K.; Wang, H.; He, S.; *et al.* Hard X-ray micro-focusing beamline at SSRF. *Nuclear Science and Techniques*, 2015, 26, 1-8.
17. Schindelin, J.; Arganda-Carreras, I.; Frise, E.; Kaynig, V.; Longair, M.; Pietzsch, T.; *et al.* Fiji: an open-source platform for biological-image analysis. *Nature Methods*, 2012, 9, 676-682.
18. Runko, A.P.; Griswold, A.J.; Min, K.T. Overexpression of frataxin in the mitochondria increases resistance to oxidative stress and extends lifespan in *Drosophila*. *FEBS Letters*, 2008, 582, 715-719.
19. Calap-Quintana, P.; Navarro, J.A.; González-Fernández, J.; Martínez-Sebastián, M.J.; Moltó, M.D.; Llorens, J.V. *Drosophila melanogaster* models of Friedreich's ataxia. *BioMed Research International*, 2018, 2018, 1-20.
20. Cabisco, E.; Tamarit, J.; Ros, J. Oxidative stress in bacteria and protein damage by reactive oxygen species. *International Microbiology: the Official Journal of the Spanish Society for Microbiology*, 2000, 3, 3-8.
21. Edenharter, O.; Clement, J.; Schneuwly, S.; Navarro, J.A. Overexpression of *Drosophila* frataxin triggers cell death in an iron-dependent manner. *Journal of Neurogenetics*, 2017, 31, 189-202.
22. Navarro, J.A.; Ohmann, E.; Sanchez, D.; Botella, J.A.; Liebisch, G.; Moltó, M.D.; *et al.* Altered lipid metabolism in a *Drosophila* model of Friedreich's ataxia. *Human Molecular Genetics*, 2010, 19, 2828-2840.
23. Sanchez-Casis, G.; Cote, M.; Barbeau, A. Pathology of the heart in Friedreich's ataxia: review of the literature and report of one case. *Canadian Journal of Neurological Sciences*, 1976, 3, 349-354.
24. Lamarche, J.B.; Cote, M.; Lemieux, B. The cardiomyopathy of Friedreich's ataxia morphological observations in 3 cases. *Canadian Journal of Neurological Sciences*, 1980, 7, 389-396.
25. Harding, I.H.; Raniga, P.; Delatycki, M.B.; Stagnitti, M.R.; Corben, L.A.; Storey, E.; *et al.* Tissue atrophy and elevated iron concentration in the extrapyramidal motor system in Friedreich ataxia: The IMAGE-FRDA study. *Journal of Neurology, Neurosurgery & Psychiatry*, 2016, 87, 1260-1263.
26. Boddaert, N.; Sang, K. H. L. Q.; Rötig, A.; Leroywillig, A.; Gallet, S.; Brunelle, F.; *et al.* Selective iron chelation in Friedreich ataxia: Biologic and clinical implications. *Blood*, 2007, 110, 401-408.
27. Shidara, Y.; Hollenbeck, P.J. Defects in mitochondrial axonal transport and membrane potential without increased reactive oxygen species production in a *Drosophila* model of Friedreich ataxia. *Journal of Neuroscience*, 2010, 30, 11369-11378.
28. Lupoli, F.; Vannocci, T.; Longo, G.; Nicolai, N.; Pastore, A. The role of oxidative stress in Friedreich's ataxia. *FEBS Letters*, 2018, 592, 718-727.
29. Edenharter, O.; Schneuwly, S.; Navarro, J.A. Mitofusin-dependent ER stress triggers glial dysfunction and nervous system degeneration in a *Drosophila* model of Friedreich's ataxia. *Frontiers in Molecular Neuroscience*, 2018, 11, 38.
30. Calap-Quintana, P.; Soriano, S.; Llorens, J.V.; Al-Ramahi, I.; Botas, J.; Moltó, M.D.; *et al.* TORC1 inhibition by rapamycin promotes antioxidant defences in a *Drosophila* model of Friedreich's ataxia. *PLoS ONE*, 2015, 10(7), e0132376.

31. Soriano, S.; Calap-Quintana, P.; Llorens, J.V.; Al-Ramahi, I.; Gutiérrez, L.; Martínez-Sebastián, M.J.; *et al.* Metal homeostasis regulators suppress FRDA phenotypes in a *Drosophila* model of the disease. *PLoS ONE*, 2016, 11, e0159209.
32. Anderson, P.R.; Kirby, K.; Orr, W.C.; Hilliker, A.J.; Phillips, J.P. Hydrogen peroxide scavenging rescues frataxin deficiency in a *Drosophila* model of Friedreich's ataxia. *Proceedings of the National Academy of Sciences of the United States of America*, 2008, 105, 611–616.
33. Macevilly, C.J.; Muller, D.P. Oxidative stress does not appear to be involved in the aetiology of Friedreich's ataxia. *Restorative Neurology and Neuroscience*, 1997, 11, 131–137.
34. Seznec, H.; Simon, D.; Bouton, C.; Reutenauer, L.; Hertzog, A.; Golik, P.; *et al.* Friedreich ataxia: the oxidative stress paradox. *Human Molecular Genetics*, 2005, 14, 463–474.
35. Monnier, V.; Llorens, J.V.; Navarro, J.A. Impact of *Drosophila* models in the study and treatment of Friedreich's ataxia. *International Journal of Molecular Sciences*, 2018, 19, 1989.

Disclaimer/Publisher's Note: The statements, opinions and data contained in all publications are solely those of the individual author(s) and contributor(s) and not of MDPI and/or the editor(s). MDPI and/or the editor(s) disclaim responsibility for any injury to people or property resulting from any ideas, methods, instructions or products referred to in the content.